Journal of Applied Physics ARTICLE scitation.org/journal/jap

Molecular dynamics simulations of thermal conductivity between two nanoparticles in contact

Cite as: J. Appl. Phys. **127**, 224303 (2020); doi: 10.1063/5.0004117
Submitted: 7 February 2020 · Accepted: 22 May 2020 ·
Published Online: 8 June 2020

G. Mora-Barzaga,[1,2,a)] E. N. Miranda,[2,3] and E. M. Bringa[1,2,4]

AFFILIATIONS

[1]CONICET, Facultad de Ingeniería, Universidad de Mendoza, Mendoza 5500, Argentina
[2]FCEN, Universidad Nacional de Cuyo, Mendoza 5500, Argentina
[3]IANIGLA, CONICET, Mendoza 5500, Argentina
[4]Centro de Nanotecnología Aplicada, Facultad de Ciencias, Universidad Mayor, Santiago 8580745, Chile

[a)]**Author to whom correspondence should be addressed:** gmorabarzaga92@gmail.com

ABSTRACT

The nanoscale properties of materials can have a great influence on their macroscopic behavior; for instance, the generation and accumulation of defects at the nanoscale, such as point defects, porosity, and interfaces, can change their thermal properties. In this work, we study the role of an interface in the thermal conductivity between two nanoparticles without any external load. We consider a system subjected to a temperature gradient perpendicular to the contact surface and study the thermal conductivity, thermal conductance, thermal resistance, and contact resistance vs nanoparticle size. The thermal resistance at the interface increases linearly with nanoparticles' contact radius a_c. A model based on the contact area between two nanoparticles allows us to reasonably explain the obtained numerical results for the thermal conductivity, leading to a net decrease in effective conductivity as the nanoparticle size increases, reasonably well described by a (a_c/R) dependence. Simulated thermal conductance was found to be proportional to (a_c/R).

I. INTRODUCTION

Nanoscale physics has been in the focus of the scientific community during the last few decades, and many theories and experiments have been formulated to explain and study the behavior of materials at this scale. However, many questions remain unanswered, including questions related to the thermodynamics properties of nanostructures. In particular, several experimental methods have been developed in order to study the thermal conductivity at the nanoscale,[1] such as the 3ω method, scanning thermal microscopy, optical pump-probe methods, and thermal conductivity spectroscopy. While these techniques have successfully measured the thermal conductivity of multiple nanostructured materials,[2,3] discrepancies have been found with models describing heat transport across interfaces.[4–6]

Previous experimental works have shown the impact of interfaces and defects on thermal properties,[6–11] creating a need for more effective and accurate calculation methods. Microscopic models can be used,[12] but defects are difficult to introduce reliably. In light of this problem, classical molecular dynamics (MD) simulations have been extensively used for studies of thermal transport at the nanoscale, especially if heat conduction is due to atomic vibrations and electronic contributions can be neglected.[8,9,13–15]

Over the last few decades, two different methods to calculate thermal conductivity have gained popularity in the scientific community:[16] the Green–Kubo formulation[17] and the direct method (direct application of Fourier's law). In this work, Non-Equilibrium Molecular Dynamics (NEMD) simulations are used to apply the direct method approach, imposing a temperature gradient across an interface in a nanostructure.

Thermal properties at the nanoscale are important for technological applications. For instance, the figure of merit of thermoelectric materials increases as the conductivity decreases.[18] In the case of nanoscale granular materials, thermal conductivity is reduced by the porosity of the material and also by the fact that the contact size is comparable to phonon mean free paths.[19] Previous

theoretical work[12,19,20] has found nanoparticles system thermal conductivity to be one or two orders of magnitude lower than in bulk, smaller than the minimum thermal conductivity given by the Einstein limit[21] and showing great promise as thermal insulators. The role of porosity on thermal conductivity has been studied extensively at the micro- and macroscale.[9,22–25] Nanoscale porosity also has been studied for Si and SiO_2.[9,26] There are many studies of heat transport across interfaces. For instance, Choi and Roberts[27] studied thermal conductance for solid Ar with a grain boundary, and Maiti *et al.*[28] and Schelling *et al.*[16] studied Kapitza resistance across grain boundaries in silicon using NEMD simulations. The role of finite size effects has been less explored. Meng *et al.*[19] studied the amorphous SiO_2 nanoparticle conductivity and the thermal resistance, showing that the interparticle resistance depends strongly on the forces between particles, in particular, the presence or absence of chemical bonds between nanoparticles.

II. METHODS

A. NEMD setup

Simulations are performed with the Large-scale Atomic/Molecular Massively Parallel Simulator[29] (https://lammps.sandia.gov). Time integration was carried out with a velocity-Verlet algorithm, with a time step of $0.005\,\tau$. The simulated system consists of two spherical fcc (face-centered cubic) nanoparticles in contact, with atoms interacting through a Lennard–Jones (LJ) potential, with a cutoff of $2.5\,\sigma$. A summary of LJ units appears in Table I.

In order to study the contact between two large atomistic spheres, we simulate only a fraction of them around the contact region. Spherical caps are created separately cutting them from the fcc single crystal, oriented to give a (001) contact plane. Caps are relaxed with the Polak–Ribiere version of the conjugate gradient (CG) algorithm in LAMMPS. Caps are then moved together such that both are within the cutoff of the potential; the system is once again relaxed with CG. During this process, the spheres come together naturally, forming a contact, as seen in Fig. 1. Both spheres share the same orientation, since we are interested in the contact finite size and not in the thermal resistance due to a grain boundary. For spheres with a radius larger than $70\,\sigma$, the contact stress is enough to nucleate dislocations, resulting in a dislocation forest at the interface, which would affect thermal conductivity and those cases have also been neglected.

In this paper, we focus on heat conduction between two spheres with the same radius, as it has been considered in most studies.[20,23] Heat conduction between unequal spheres might also be of interest, especially given that under experimental conditions, there is usually a size distribution involved.[10,30] For spheres of radius R_1 and R_2, the effective radius of the system is

$$R_{eff} = \frac{2R_1R_2}{R_1 + R_2}.$$

Results related to contact mechanics for two spheres with the same radius R should be equivalent to results for two spheres of different individual radii if $R_{eff} = R$. In order to consider this scenario, we also include a few heat conduction simulations for spheres where one has a radius of $23\,\sigma$, and the other has a radius of 17, 20, or $27\,\sigma$. We note that, instead of R_{eff}, $R^* = R_{eff}/2$ is often used in contact models.

TABLE I. Table of LJ units.

Magnitude	Units	Magnitude	Units
Mass	m	Force	ϵ/σ
Distance	σ	Temperature	ϵ/k_B
Energy	ϵ	Pressure	ϵ/σ^3
Time (τ)	$(\epsilon/m/\sigma^2)^{-1/2}$	Density	σ^{-3}
Velocity	σ/τ		

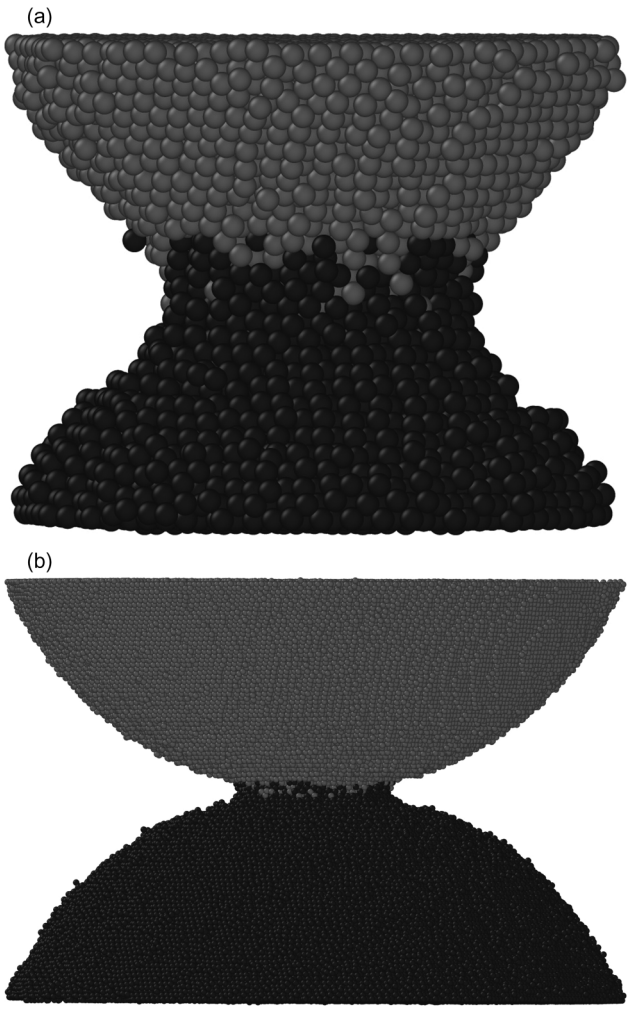

FIG. 1. Slices of the nanoparticle system at the end of the simulation, for T = 0.4, and for different radius, R, of the spheres. (a) $R = 17\,\sigma$ and (b) $R = 60\,\sigma$. Shades of gray represent the atoms of the different nanoparticles, as classified at the beginning of the simulation.

B. Contact radius

Previous work[19,31–33] showed the importance of the contact radius(a_c) in the estimation of thermal properties.

Johnson–Kendall–Roberts (JKR),[34] and Derjaguin, Muller, and Toporov (DMT)[35] derived expressions for the contact radius between two elastic, adhesive spheres. For zero external pressure, which is the case studied here,

$$a_{JKR} = \left[\left(\frac{9}{4}\right)\left(\frac{\gamma\pi R^2}{E^*}\right)\right]^{1/3} \tag{1}$$

and

$$a_{DMT} = \frac{4}{3}a_{JKR}, \tag{2}$$

where R is the nanoparticle radius, E^* the reduced elastic modulus, and γ is the surface energy. $E^* = \left[(1-\nu_1^2)/E_1 + (1-\nu_2^2)/E_2\right]^{-1}$ depends on the elastic module E and the Poisson coefficient ν of the nanoparticles.

The Tabor parameter[36] is defined by

$$\mu = \left(\frac{R\omega^2}{2E^{*2}z^3}\right)^{1/3}, \tag{3}$$

where ω is the work of adhesion and z the equilibrium separation between the spheres. μ was found to be between 0.4 and 0.7 for our system, which, according to Johnson and Greenwood,[36] lies in the region between the two models.

In our simulation, a_c was calculated using the relation proposed by Vergeles *et al.*,[37]

$$a_c^2 = \sum_{i=1}^{N}\frac{(x_i - x_c)^2 + (y_i - y_c)^2}{N}, \tag{4}$$

where the summation is over all N atoms with $z_i = z_c \pm 0.5\sigma$. z_c is the location where the spheres touch, and x_c and y_c are the coordinates of the center of mass of the N atoms. Contact radius was also calculated using the scientific visualization and analysis software OVITO[38] (https://ovito.org), using the SurfaceMesh utility.

Figure 2 shows contact radius vs radius of the nanoparticle, according to the DMT and JKR models, and from our simulations, using the two different methods mentioned above. The agreement between the Vergeles and OVITO approach was excellent. As expected from the models, results are closer to the DMT prediction at small radii, when cohesive forces are relatively stronger, and results approach the JKR prediction as the radius increases. This is related to the increase of the Tabor parameter μ,[36] given by Eq. (3). Due to this transitional behavior, the relationship $a_c \propto R^{1/2}$ gives a better fit than $a_c \propto R^{2/3}$ predicted by Eqs. (1) and (2). The effective contact radii for unequal spheres also agree with DMT/JKR models, as expected.

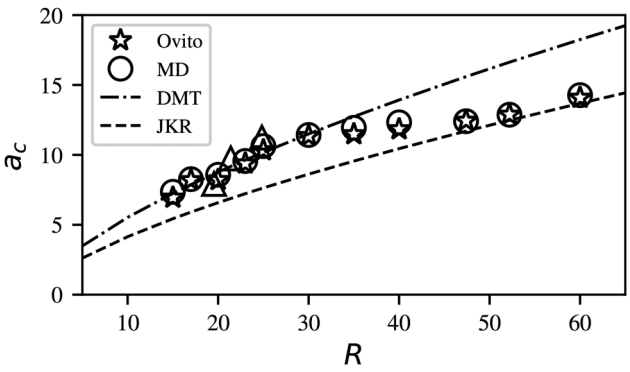

FIG. 2. Contact radius a_c vs R. The dashed and dashed-dotted lines were obtained from Eqs. (1) and (2), respectively, Young's modulus, surface energy, and Poisson coefficient were chosen according to Quesnel *et al.*[39] Results for unequal spheres, using OVITO, are shown as triangles.

C. Thermal conductivity calculation

There are many methods to calculate thermal conductivity, k_{eff}, at the nanoscale,[9] including methods that can distinguish different heat propagation modes.[40] Here, we require a method that can handle non-periodic boundary conditions, and up to nearly 10^6 atoms. Due to these limitations, we use the direct method, with non-equilibrium molecular dynamics (NEMD) simulations of a temperature gradient[41] across the interface and also across the nanoparticles.[19] Fourier's law can be applied,

$$k_{eff} = J\Delta z/\Delta T,$$

where $J = Q/(A_t t)$ and $\Delta T/\Delta z$ are the heat flux (Fig. 3) and the temperature gradient across the system (Fig. 4). A_t, Q, and t are the thermostated area, the heat supplied by the thermostat, and time. We calculate thermal conductivity only after a steady state has been

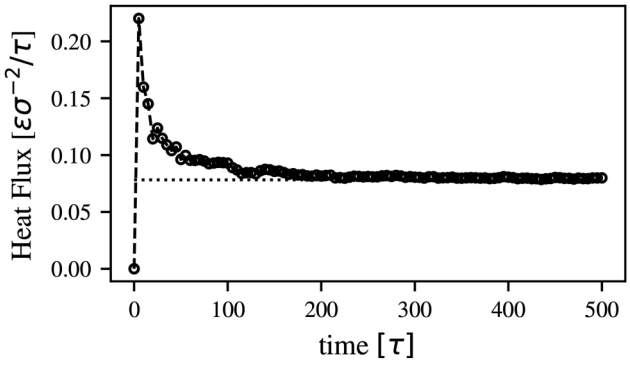

FIG. 3. Representative case for heat flux vs time, corresponding to the case of two equal spheres, with R = 30 σ. Heat flux becomes steady after 200 LJ time units (420 ps for Ar). The dotted line indicates the value used to calculate thermal conductivity for this case, T = 0.4.

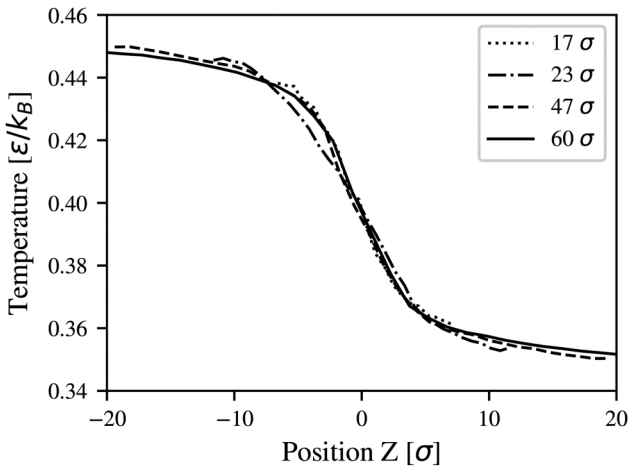

FIG. 4. Temperature profiles for different nanoparticles radii averaged over the last 10^6 simulation steps (approximately 1 ns for Ar), T = 0.4.

reached for both the heat flux, as seen in Fig. 3, and for the temperature gradient.

A thin, fix region with a width of 2σ is set at the far end of each of the caps, and then a Langevin thermostat is applied during 10^5 steps, such that all the system achieves a desired temperature. In this work, we use T = 0.4 (approximately 40 K for Ar). At the end of the thermalization, the system is still nearly stress free at the interface, so the comparison with models for zero contact pressure is valid. The lattice parameter is $a_0 = 1.56$ at this finite temperature. Some atomic mixing occurs at the interface for the smaller nanoparticles, as observed in Fig. 1(a). A temperature gradient is then applied to calculate thermal transport. Regions with a width 3σ next to each fix region of the simulation box are set to $T - \delta$ and $T + \delta$, respectively, during 3 10^6 steps. δ was typically set to 5% of the target temperature. Thermal and physical properties of the system were calculated every 10^4 steps, and averaged over the following 10^6 steps. We note that the contact radius is not modified by the application of the temperature gradient.

The Langevin thermostat enables the calculation of the cumulative energy added/subtracted to the atoms as they are thermostated during the simulation. Effectively, this gives the energy exchanged between an infinite thermal reservoir and the nanoparticles. Then, Q can be calculated as the average between the energy added and subtracted to the hot and cold thermostat, respectively. Before calculating the conductivity for a nanosystem, the method was validated using bulk calculations. Table II shows that our results for bulk Argon(Ar) are in good agreement with experiments and MD bulk simulations.[27,42]

Several methods have been proposed to predict the effective thermal conductivity of a random packing of spheres.[23,45–47] In this work, we use the expression that Argento and Bouvard[23] derived from Carslaw *et al.*[46] analysis, for the normalized thermal conductivity,

$$\frac{k_{eff}}{k_{bulk}} = \frac{1}{\pi R}\rho n_c a_c, \tag{5}$$

TABLE II. Results for bulk argon (Ar), including experiments (*k*-Expt.[43]) and previous MD simulations, MD-1,[27] MD-2,[42] and MD-3,[44] showing that our method provides adequate conductivity values for a bulk system. Temperature is given in K and thermal conductivity in W/(K m).

T (K)	*k*-Expt.	*k*-MD-1	*k*-MD-2	*k*-MD-3	*k*-MD
10	3.67	2.36	4	3.33	3.15
20	1.36		1.57		1.58
25	0.99	1.05			1.08
30	0.78		0.903	0.87	0.905
50	0.46	0.53	0.417		0.45

where n_c is the mean number of contacts per particle and ρ is the relative density of the packing.

D. The Einstein thermal conductivity limit

Assuming the phonon mean free path equal to half the wavelength of the phonons, Einstein calculated the lowest possible thermal conductivity of a solid, k_{Eins}.[48] This model, known as the Einstein limit, gives conductivity values, which are extremely low for crystalline solids,[21,49] where the mean free path can be more than one order of magnitude longer that Einstein assumed. However, the model has been used to roughly explain the thermal conductivity of amorphous solids, where there are no coherent vibrations.[21] k_{Eins} can be calculated as[21]

$$k_{Eins} = \frac{k_B^2}{\hbar}\frac{n^{1/3}}{\pi}\Theta_E\frac{x^2e^x}{(e^x-1)^2}, \tag{6}$$

where $n = a_0^{-3}$ is the number density of atoms, Θ_E is the Einstein temperature, and $x = \Theta_E/T$. $\Theta_E = \frac{\hbar}{k_B}\sqrt{\frac{K}{m}}$ for a harmonic solid with atoms of mass m and spring constant K. For LJ systems,[50] $K = \frac{72\epsilon}{2^{1/3}\sigma^2}$, and we use $n = 4a_0^{-3}$ for fcc solids. Prasher[20] theoretical analysis for a bed of nanoparticles found thermal conductivity values below the Einstein limit. MD simulations[51] for a LJ solid show that the effective phonon mean free path at T = 0.4 is close to 10σ, while the Einstein limit calculation, Eq. (6), considers the phonon mean free path close to 1σ.[21] This increased mean free path would lead to a much better agreement between k_{Eins} and our bulk MD simulations. In this work, MD conductivity results for two spheres are also compared to Einstein limit value.

E. Contact resistance and thermal conductance

Due to the presence of an interface, determining the effective thermal conductivity of a system is intrinsically related to the thermal boundary resistance or contact resistance (R_K)[52] and also to the thermal boundary conductance (TC). R_K and TC are calculated using NEMD as

$$R_K = \frac{1}{TC} = \frac{\Delta T_c}{J_c},$$

where $J_c = Q/(A_c t)$ and ΔT_c are the heat flux and temperature-drop at the interface. A_c is the interface contact area. Figure 5 illustrates how ΔT_c was calculated.

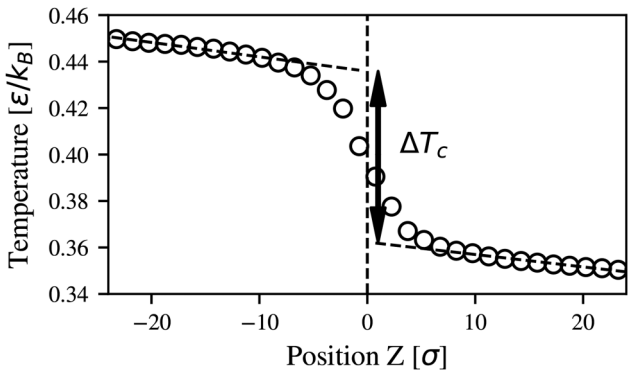

FIG. 5. Temperature drop ΔT_c at the interface between the nanoparticles. The arrows show the magnitude of ΔT_c used in the calculation of the contact resistance.

F. Thermal resistance

Another interesting property is the one-dimensional thermal resistance

$$R_T = \frac{\Delta T}{\dot{Q}},$$

where $\dot{Q}$ is the heat flow or heat rate (Q/t). R_T only considers the heat rate and the temperature drop imposed by that heat rate. This facilitates experimental measurements, compared to the contact resistance, due to the difficulties obtaining an accurate experimental contact area in a nanoscale system.[11,23]

For the bulk, the thermal resistance can be found as

$$R_T^{bulk} = \frac{\Delta z}{A_t k_{bulk}},$$

where Δz and A_t represent the dimension and the cross section area in the heat transfer direction, respectively.

According to Carslaw *et al.*[46] analysis, the thermal resistance for our specific geometry can be predicted as

$$\frac{R_{cyl}}{R_T} = \frac{4}{\pi}\left(\frac{a_c}{R}\right), \tag{7}$$

where R_{cyl} is R_T^{bulk} for a cylinder with a height equal to the distance between both cold and hot thermostat, and a cross section equal to the thermostated area.

Argento and Bouvard,[23] using a finite element code, found this relationship to be

$$\frac{R_{cyl}}{R_T} = 1.112\left(\frac{a_c}{R}\right). \tag{8}$$

We note that they use the same particle radius and modify contact radius by applying external pressure.

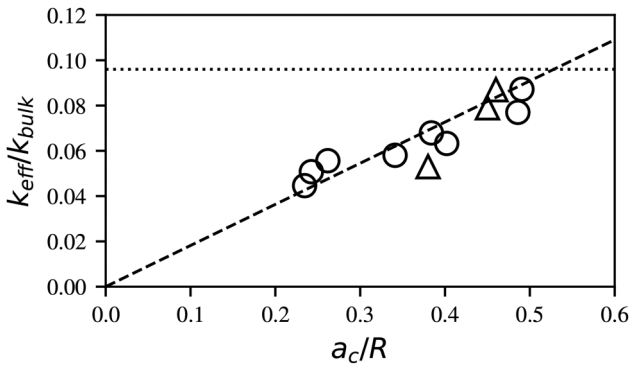

FIG. 6. Thermal conductivity vs normalized contact radii (a_c/R). The dashed line shows Eq. (5) for a single contact, $n_c = 1$. The dotted line is the Einstein conductivity value for T = 0.4. Includes results for unequal spheres (triangles), using $R = R_{eff}$.

III. RESULTS AND DISCUSSION

A. Thermal conductivity

k_{eff} was calculated using the methodology outlined in Sec. II. Figure 6 shows the behavior of the normalized thermal conductivity vs (a_c/R). Results show that the conductivity of the system is between 4% and 10% of the bulk conductivity and, as predicted in Prasher[20] analysis, is even smaller than the Einstein limit for bulk conductivity. Note that the contact diameter $(2a_c)$ between the nanospheres in our simulations, Fig. 2, was always larger, but similar, to the phonon mean free path $(10\,\sigma)$ for the temperature studied here.[51]

Equation (5) was fitted using a single contact, $n_c = 1$, corresponding to the geometry in our simulations from Fig. 1. MD results agree surprisingly well with Eq. (5), given that the model was not developed for the nanoscale. Since $\frac{k_{eff}}{k_{bulk}} \propto (a_c/R)$ and, for this nanoparticle size range, $a_c \propto R^{1/2}$ (see Subsection II B), Fig. 7

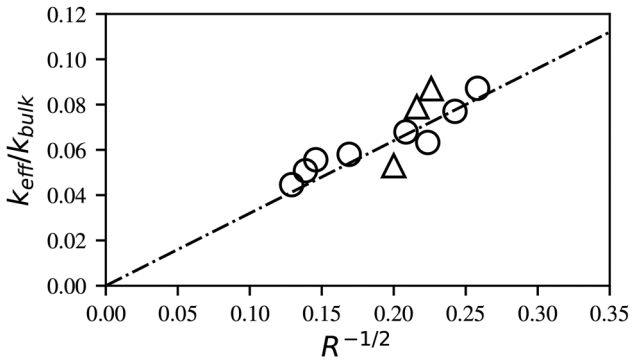

FIG. 7. Thermal conductivity vs $R^{-1/2}$ for T = 0.4. The dashed line shows the relation $\frac{k_{eff}}{k_{bulk}} = 0.32R^{-1/2}$. Includes results for unequal spheres (triangles), using $R = R_{eff}$.

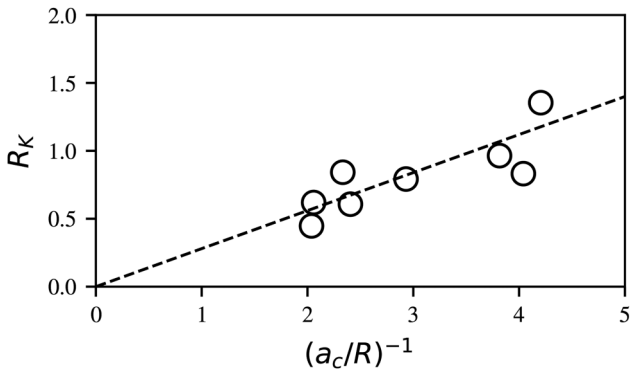

FIG. 8. Contact resistance vs the inverse of the normalized contact radii (a_c/R). The dashed line shows $R_k = 0.28\left(\frac{a_c}{R}\right)^{-1}$. For Ar, it would be R_K (1.9 K m^2/GW).

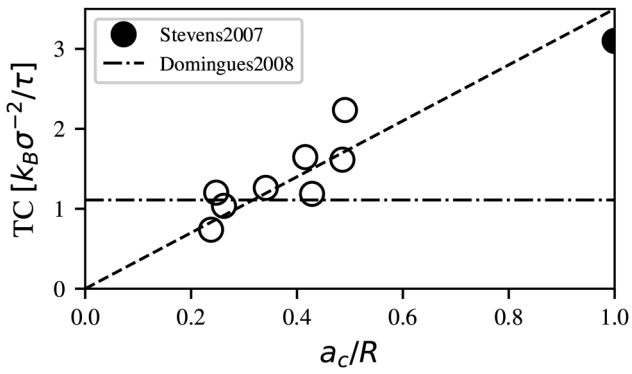

FIG. 10. Thermal conductance (TC) vs (a_c/R). A linear fit to the MD results, $TC = 3.5\left(\frac{a_c}{R}\right)$, has been added to guide the eye. The dotted-dashed line shows the results from Domingues *et al.*[55] The black dot shows the bulk result from Stevens *et al.*[41]

shows that the relationship $\frac{k_{eff}}{k_{bulk}} \propto R^{-1/2}$ fits our results fairly well, as expected. The conductivity for a system of unequal spheres also follows reasonably well the results for equal-size spheres.

B. Thermal and contact resistance

Figure 8 shows the MD results obtained for R_K, where a linear relationship was found between R_K and $\left(\frac{a_c}{R}\right)^{-1}$. Taking into account that $a_c \propto R^{1/2}$ for this size range, a linear relationship could be considered for R_K vs a_c. These values of thermal resistance are in the same order of magnitude as those determined in previous MD simulations of Kapitza resistance across interfaces in Si[28,53] or Si/SiO_2.[54]

For the thermal resistance, we found that

$$\frac{R_{cyl}}{R_T} = 0.92\left(\frac{a_c}{R}\right), \tag{9}$$

where $\frac{R_{cyl}}{R_T} \propto \left(\frac{a_c}{R}\right)$, but the slope was smaller than the ones predicted from Eqs. (7) and (8). Figure 9 shows a comparison between our results and the results of Carslaw *et al.*[46] and Argento and Bouvard.[23]

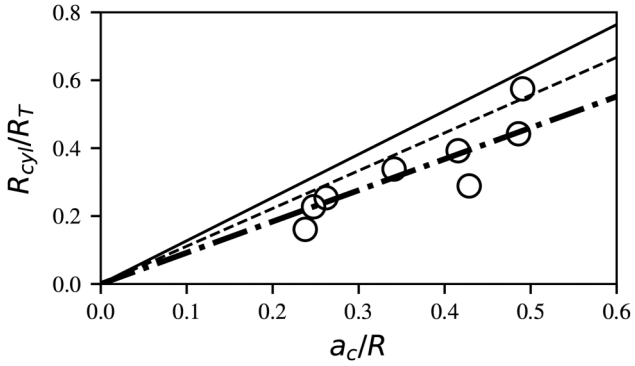

FIG. 9. Normalized inverse thermal resistance vs normalized contact radius. Lines show the predictions for Eq. (7) (solid line), Eq. (8) (dashed line), and Eq. (9) (dotted-dashed line).

C. Thermal conductance

Thermal boundary conductance (TC)[11,41] is defined as $TC = 1/R_K$. Therefore, from Fig. 8, TC would be proportional to (a_c/R). Conductance is, therefore, proportional to the contact radius, increasing with the number of atoms in the contact region, as shown in Fig. 10. For a bulk LJ system, TC was found to be $TC \approx 3.1$.[41] This is consistent with our results if we take the bulk system conditions equivalent to the ones for $(a_c/R) = 1$. TC for unequal spheres was not calculated due to difficulties calculating the heat flux through the contact area: lack of symmetry along the heat propagation direction, perpendicular to the contact interface, causes heat flux variations alongside that direction.

Domingues *et al.*[55] calculated TC between silica nanoparticles ($R = 0.75$–2.5 nm) from fluctuations in the heat flux from MD simulations. Thermal conductance fluctuated significantly, and results were transformed to an "atomic conductance," multiplying TC by the contact area. This "atomic conductance," TC_a, had units of (W/K) and it was found to be roughly proportional to contact surface. They proposed an estimation of this atomic conductance as $TC_a = (9/8)k_B N_c/\tau$, where N_c is the number of atoms involved in heat transfer at the interface, and $1/\tau \approx \omega$ was estimated from the largest phonon frequency for the system. We use the Debye frequency for LJ, $\omega = 0.976$, and use contact area equal to $N_c a_{at}$, where for LJ and the density in our simulations, $a_{at} = 0.98\sigma^2$. This gives $TC = 1.11$, within the range of the values found in the simulation, which indicates excellent agreement with our results, given the simplicity of the analytical approximation.

IV. CONCLUSIONS

Thermal properties of two spherical nanoparticles in contact have been studied considering Lennard–Jones interactions and no external pressure. There is a transition between the Johnson–

Kendall–Roberts (JKR)[34] and Derjaguin, Muller, and Toporov (DMT)[35] models for the nanoparticle contact radius at the studied scales, as expected.[36] Due to this transition, the dependence of a_c with R is better described by $R^{1/2}$, and not $R^{2/3}$, as it is usually assumed from a single model.

A thermal gradient was applied across the system, and the steady-state heat flux was measured for different configurations. Bulk thermal conductivity simulations used to calibrate our methodology show good agreement with experiments and previous MD simulations.

Thermal conductivity between two spheres in contact decreases with the contact radius a_c, and also decreases with nanoparticle radius R. On the other hand, thermal conductivity increases with the ratio (a_c/R) and is better described by (a_c/R), not by a_c or R alone. It was found that a simple model based on the contact area between spheres[23] can reasonably explain this behavior of the thermal conductivity.

We have also simulated unequal spheres and find that thermal transport can be well described by the models and fits for equal-size spheres, if the effective radius of the system is considered.

Temperature inside the nanoparticles varies relatively slowly, but there is a large temperature drop at their interface, and the contact resistance associated with this drop increases linearly with the contact radius a_c and decreases with (a_c/R). Macroscopic models for thermal resistance based on (a_c/R)[23] show good agreement with our nanoscale MD results.

Simulated thermal conductance was found to be directly proportional to (a_c/R). Values are consistent with previous simulated bulk values[41] and with a simple analytical model.[55]

The values found for the nanoparticles thermal conductivity were below the Einstein limit for bulk conductivity,[21] as predicted by Prasher,[20] despite considering here only a "perfect" interface between nanoparticles with the same type of atoms. Therefore, our low values for the thermal conductivity of the nanosystem could be decreased even further by changing the conditions at the nanoparticle interface, which shows the potential of nanoparticles systems as insulators.

At the temperature studied here, $T = 0.4$, the phonon mean free path is slightly smaller than the contact diameter. Simulations at lower temperature, where the mean free path is significantly larger,[51] might provide a larger reduction of the conductivity with respect to bulk values.

It would be useful to consider in future studies the role of contact pressure in the modification of thermal conductivity. Compressive pressure would increase the contact radius,[34] but also add lattice strain, which can modify phonon transport,[15] and possibly nucleate pressure-induced defects.

Future research might also include the role of defects in the nanoparticles, such as dislocations and vacancies, which would influence thermal conductivity, especially if they are near or at the interface, likely leading to a further decrease in thermal transport.

ACKNOWLEDGMENTS

We acknowledge the CONICET for financial support. E.M.B. acknowledges support from the SIIP-UNCuyo 06/M104 grant. G.M.-B. acknowledges the SiMAF group for helpful discussions. This work used the Toko Cluster from FCEN-UNCuyo, which is part of the SNCAD-MinCyT, Argentina.

DATA AVAILABILITY

The data that support the findings of this study are available from the corresponding author upon reasonable request.

REFERENCES

[1]T. Luo and G. Chen, "Nanoscale heat transfer–from computation to experiment," Phys. Chem. Chem. Phys. **15**(10), 3389–3412 (2013).
[2]M. T. Barako, S. Roy-Panzer, T. S. English, T. Kodama, M. Asheghi, T. W. Kenny, and K. E. Goodson, "Thermal conduction in vertically aligned copper nanowire arrays and composites," ACS Appl. Mater. Interfaces **7**(34), 19251–19259 (2015).
[3]M. Ruoho, K. Valset, T. Finstad, and I. Tittonen, "Measurement of thin film thermal conductivity using the laser flash method," Nanotechnology **26**(19), 195706 (2015).
[4]R. J. Stoner and H. J. Maris, "Kapitza conductance and heat flow between solids at temperatures from 50 to 300 K," Phys. Rev. B **48**(22), 16373 (1993).
[5]R. J. Stevens, A. N. Smith, and P. M. Norris, "Measurement of thermal boundary conductance of a series of metal–dielectric interfaces by the transient thermoreflectance technique," J. Heat Transfer **127**(3), 315–322 (2005).
[6]P. E. Hopkins, P. M. Norris, R. J. Stevens, T. E. Beechem, and S. Graham, "Influence of interfacial mixing on thermal boundary conductance across a chromium/silicon interface," J. Heat Transfer **130**(6), 062402 (2008).
[7]P. E. Hopkins, "Thermal transport across solid interfaces with nanoscale imperfections: Effects of roughness, disorder, dislocations, and bonding on thermal boundary conductance," ISRN Mech. Eng. **2013**, 1–19.
[8]D. G. Cahill, W. K. Ford, K. E. Goodson, G. D. Mahan, A. Majumdar, H. J. Maris, R. Merlin, and S. R. Phillpot, "Nanoscale thermal transport," J. Appl. Phys. **93**(2), 793–818 (2003).
[9]D. G. Cahill, P. V. Braun, G. Chen, D. R. Clarke, S. Fan, K. E. Goodson, P. Keblinski, W. P. King, G. D. Mahan, A. Majumdar, H. J. Maris, S. R. Phillpot, E. Pop, and L. Shi, "Nanoscale thermal transport. II. 2003–2012," Appl. Phys. Rev. **1**(1), 011305 (2014).
[10]Y. Liang and X. Li, "A new model for heat transfer through the contact network of randomly packed granular material," Appl. Therm. Eng. **73**(1), 984–992 (2014).
[11]A. Giri and P. E. Hopkins, "A review of experimental and computational advances in thermal boundary conductance and nanoscale thermal transport across solid interfaces," Adv. Funct. Mater. **30**(8), 1–21 (2020).
[12]R. Prasher, "Predicting the thermal resistance of nanosized constrictions," Nano Lett. **5**(11), 2155–2159 (2005).
[13]N. A. Roberts, D. G. Walker, and D. Y. Li, "Molecular dynamics simulation of thermal conductivity of nanocrystalline composite films," Int. J. Heat Mass Transf. **52**(7–8), 2002–2008 (2009).
[14]K. Termentzidis, S. Merabia, P. Chantrenne, and P. Keblinski, "Cross-plane thermal conductivity of superlattices with rough interfaces using equilibrium and non-equilibrium molecular dynamics," Int. J. Heat Mass Transf. **54**(9–10), 2014–2020 (2011).
[15]R. C. Picu, T. Borca-Tasciuc, and M. C. Pavel, "Strain and size effects on heat transport in nanostructures," J. Appl. Phys. **93**(6), 3535–3539 (2003).
[16]P. K. Schelling, S. R. Phillpot, and P. Keblinski, "Comparison of atomic-level simulation methods for computing thermal conductivity," Phys. Rev. B **65**(14), 1–12 (2002).
[17]W. Lv and A. Henry, "Direct calculation of modal contributions to thermal conductivity via Green–Kubo modal analysis," New J. Phys. **18**(1), 013028 (2016).
[18]L. Lindsay, A. Katre, A. Cepellotti, and N. Mingo, "Perspective on *ab initio* phonon thermal transport," J. Appl. Phys. **126**(5), 050902 (2019).

[19]F. Meng, M. Elsahati, J. Liu, and R. F. Richards, "Thermal resistance between amorphous silica nanoparticles," J. Appl. Phys. **121**(19), 194302 (2017).
[20]R. Prasher, "Ultralow thermal conductivity of a packed bed of crystalline nanoparticles: A theoretical study," Phys. Rev. B **74**(16), 1–5 (2006).
[21]D. G. Cahill and R. O. Pohl, "Heat flow and lattice vibrations in glasses," Solid State Commun. **70**(10), 927–930 (1989).
[22]T. H. Bauer, "A general analytical approach toward the thermal conductivity of porous media," Int. J. Heat Mass Transf. **36**(17), 4181–4191 (1993).
[23]C. Argento and D. Bouvard, "Modeling the effective thermal conductivity of random packing of spheres through densification," Int. J. Heat Mass Transf. **39**(7), 1343–1350 (1996).
[24]J. K. Carson, S. J. Lovatt, D. J. Tanner, and A. C. Cleland, "Thermal conductivity bounds for isotropic, porous materials," Int. J. Heat Mass Transf. **48**(11), 2150–2158 (2005).
[25]M. Krause, J. Blum, Y. V. Skorov, and M. Trieloff, "Thermal conductivity measurements of porous dust aggregates: I. Technique, model and first results," Icarus **214**(1), 286–296 (2011).
[26]P. E. Hopkins, B. Kaehr, L. M. Phinney, T. P. Koehler, A. M. Grillet, D. Dunphy, F. Garcia, and C. Jeffrey Brinker, "Measuring the thermal conductivity of porous, transparent SiO_2 films with time domain thermoreflectance," J. Heat Transfer. **133**(6), 61601 (2011).
[27]C. J. Choi and N. Roberts, "Contributions of mass and bond energy difference and interface defects on thermal boundary conductance," AIP Adv. **5**(9), 097160 (2015).
[28]A. Maiti, G. D. Mahan, and S. T. Pantelides, "Dynamical simulations of nonequilibrium processes—Heat flow and the Kapitza resistance across grain boundaries," Solid State Commun. **102**(7), 517–521 (1997).
[29]S. Plimpton, "Fast parallel algorithms for short-range molecular dynamics," J. Comp. Phys. **117**, 1–19 (1995).
[30]A. B. Duncan, G. P. Peterson, and L. S. Fletcher, "Effective thermal conductivity within packed beds of spherical particles," J. Heat Transfer **111**(4), 830 (1989).
[31]R. Prasher, "Thermal interface materials: Historical perspective, status, and future directions," Proc. IEEE **94**(8), 1571–1586 (2006).
[32]H. Xiang, P.-X. Jiang, and Q.-X. Liu, "Non-equilibrium molecular dynamics study of nanoscale thermal contact resistance," Mol. Simul. **34**(2013), 679–687 (2008).
[33]E. Barthel, "Adhesive elastic contacts: JKR and more," J. Phys. D Appl. Phys. **41**(16), 163001 (2008).
[34]K. L. Johnson, K. Kendall, and A. D. Roberts, "Surface energy and the contact of elastic solids," Proc. R. Soc. A **324**(1558), 301–313 (1971).
[35]B. V. Derjaguin, V. M. Muller, and Y. P. Toporov, "Effect of contact deformation on the adhesion of elastic solids," J. Colloid Interface Sci. **53**(2), 314–326 (1975).
[36]K. L. Johnson and J. A. Greenwood, "An adhesion map for the contact of elastic spheres," J. Colloid Interface Sci. **192**(2), 326–333 (1997).
[37]M. Vergeles, A. Maritan, J. Koplik, and J. R. Banavar, "Adhesion of solids," Phys. Rev. E **56**(3), 2626–2634 (1997).
[38]A. Stukowski, "Visualization and analysis of atomistic simulation data with OVITO—The open visualization tool," Modell. Simul. Mater. Sci. Eng. **18**(1), 015012 (2010).
[39]D. J. Quesnel, D. S. Rimai, and L. P. DeMejo, "Elastic compliances and stiffnesses of the fcc Lennard–Jones solid," Phys. Rev. B **48**(10), 6795–6807 (1993).
[40]H. R. Seyf, K. Gordiz, F. DeAngelis, and A. Henry, "Using Green–Kubo modal analysis (GKMA) and interface conductance modal analysis (ICMA) to study phonon transport with molecular dynamics," J. Appl. Phys. **125**(8), 081101 (2019).
[41]R. J. Stevens, L. V. Zhigilei, and P. M. Norris, "Effects of temperature and disorder on thermal boundary conductance at solid–solid interfaces: Nonequilibrium molecular dynamics simulations," Int. J. Heat Mass Transf. **50**(19–20), 3977–3989 (2007).
[42]A. J. H. McGaughey and M. Kaviany, "Thermal conductivity decomposition and analysis using molecular dynamics simulations. Part I. Lennard–Jones argon," Int. J. Heat Mass Transf. **47**(8–9), 1783–1798 (2004).
[43]C. Y. Ho, R. W. Powell, and P. E. Liley, "Thermal conductivity of the elements," J. Phys. Chem. Ref. Data **1**(2), 279–421 (1972).
[44]R. E. Jones, J. C. Duda, X. W. Zhou, C. J. Kimmer, and P. E. Hopkins, "Investigation of size and electronic effects on Kapitza conductance with non-equilibrium molecular dynamics," Appl. Phys. Lett. **102**(18), 1–5 (2013).
[45]A. Jagota and C. Y. Hui, "The effective thermal conductivity of a packing of spheres," J. Appl. Mech. **57**(5), 789–791 (1990).
[46]H. S. Carslow, J. C. Jaeger, and J. E. Morral, *Conduction of Heat in Solids*, 2nd ed. (Clarendon Press, Oxford, 1959).
[47]N. Wakao and D. Vortmeyer, "Pressure dependency of effective thermal conductivity of packed beds," Chem. Eng. Sci. **26**(10), 1753–1765 (1971).
[48]A. Einstein, "Elementare betrachtungen über die thermische molekularbewegung in festen körpern," Ann. Phys. **340**(9), 679–694 (1911).
[49]D. G. Cahill, S. K. Watson, and R. O. Pohl, "Lower limit to the thermal conductivity of disordered crystals," Phys. Rev. B **46**(10), 6131–6140 (1992).
[50]R. Prasher, "Acoustic mismatch model for thermal contact resistance of van der Waals contacts," Appl. Phys. Lett. **94**(4), 1–4 (2009).
[51]S. H. Choi, S. Maruyama, K. K. Kim, and J. H. Lee, "Evaluation of the phonon mean free path in thin films by using classical molecular dynamics," J. Korean Phys. Soc. **43**(5 I), 747–753 (2003).
[52]N. Goel, E. B. Webb, A. Oztekin, J. M. Rickman, and S. Neti, "Kapitza resistance at segregated boundaries in β-SiC," J. Appl. Phys. **118**(11), 115101 (2015).
[53]P. K. Schelling, S. R. Phillpot, and P. Keblinski, "Kapitza conductance and phonon scattering at grain boundaries by simulation," J. Appl. Phys. **95**(11 I), 6082–6091 (2004).
[54]S. S. Mahajan and G. Subbarayan, "Estimating Kapitza resistance between Si–SiO_2 interface using molecular dynamics simulations," IEEE Trans. Compon. Packag. Manuf. Technol. **1**(8), 1132–1139 (2011).
[55]G. Domingues, D. Rochais, and S. Volz, "Thermal contact resistance between two nanoparticles," J. Comput. Theor. Nanosci. **5**(2), 153–156 (2008).